nature photonics

Supplementary information https://doi.org/10.1038/s41566-025-01683-4

Chirality-induced quantum non-reciprocity

In the format provided by the authors and unedited

Supplementary Information for

Chirality-induced quantum nonreciprocity

Zimo Zhang†, Zhongxiao Xu†, Ran Huang†, Xingda Lu, Fengbo Zhang, Donghao Li, Şahin K. Özdemir, Franco Nori, Han Bao, Yanhong Xiao, Bing Chen*, Hui Jing*, and Heng Shen*

†These authors contributed equally to this work.

*e-mail: hengshen@nbi.dk (H.S.); jinghui@hunnu.edu.cn (H.J.); bingchenphysics@hfut.edu.cn (B.C.)

S.1 Effective Hamiltonian of our non-Hermitian optical system

Following the conventional notion of spin states[S1, S2], we use the slow-varying atomic density operator $\hat{\sigma}^{j}_{\mu\nu} = |\mu\rangle_j\langle\upsilon|$ to describe the j-th atom spin state. In particular, the atomic operator at position z in the rotating frame can be defined by locally averaging over a transverse slice containing many atoms $\hat{\sigma}_{\mu\upsilon}(z,t) = \lim_{\Delta z\to 0}\frac{L}{N\Delta z}\sum_{z<z_j<z+\Delta z}\hat{\sigma}^{j}_{\mu\upsilon}(z,t)$ with $\hat{\sigma}^{j}_{\mu\upsilon}(z,t) = |\mu\rangle_j\langle\upsilon|e^{-i\omega_{\mu\upsilon}t}$ and transition frequency $\omega_{\mu\upsilon}$. In fact, since the optical coherences $\hat{\sigma}_{31}$ and $\hat{\sigma}_{32}$ decay much faster than the ground-state coherences $\hat{\sigma}_{12}$, we can assume that they follow the slow oscillations in the ground-state coherences. Consequently, the atomic ground state coherence $\hat{\sigma}_{12}$, the so-called atomic spin wave, plays an essential role in the dissipative coupling. Regarding the conception of atomic spin wave, the energy-level structure of the atoms in the ensemble consists of the ground states $|1\rangle$ and $|2\rangle$, and the excited state $|3\rangle$ (see Fig.1 in the main text). A transition $|1\rangle\to|3\rangle$ (or $|2\rangle\to|3\rangle$) is coupled by the classical control laser, and the forward-scattered Stokes photon comes from the transition $|3\rangle\to|2\rangle$ (or $|3\rangle\to|1\rangle$), which is co-propagating with the control beam. Such scattering events are uniquely correlated with the excitation of the collective atomic mode, and this excitations in atomic ensembles can be viewed as waves of excited spins[S3].

The effective Hamiltonian of the two atomic spin waves (atomic ground state coherence) in the two channels can be described by the following Hamiltonian[S4]:

$$\mathrm{H} = \begin{pmatrix} |\Delta_0| - i\gamma_{12} & i\Gamma \\ i\Gamma & -|\Delta_0| - i\gamma_{12} \end{pmatrix}, \tag{S.1}$$

where Γ and γ_{12} are the coupling rate and the decay rate of the two spin waves, respectively. The off-diagonal coupling term is imaginary due to the random nature of the coherence transfer between the two channels via ballistic motion and wall bouncing of atoms. The eigenvalues of this anti-parity-time symmetric Hamiltonian correspond to the two eigen-modes of electromagnetically induced transparency: $\omega_{\pm} = -i\gamma_{12} \pm \sqrt{\Delta_0^2 - \Gamma^2}$, where the real and imaginary parts are the centres of electromagnetically induced transparency and corresponding linewidths, respectively. Here, γ_{12} and $|\Delta_0|$ are the common decay rate and half the frequency difference of the two spin waves, respectively. Anti-parity-time symmetry breaking occurs at the exceptional point, $|\Delta_0| = \Gamma$, where the two supermodes perfectly overlap. In the symmetry-unbroken regime ($|\Delta_0| < \Gamma$), the two centres coincide, but with different linewidths. This system enters the symmetry-breaking regime for $|\Delta_0| > \Gamma$, and the resonances bifurcate, resembling a passively coupled system. Here, we have:

$$\begin{aligned}\Delta_0 &= (\delta_{13} - \omega_{13}) - (\delta_{23} - \omega_{23}) \\ &= \omega_{23} - \omega_{13} + (m_2 g\mu B - m_1 g\mu B) \\ &= \omega_{23} - \omega_{13} + 2g\mu B \end{aligned} \tag{S.2}$$

where B is the magnetic induction intensity, g is the Landég-factor, and μ is the total magnetic moment. Here, δ_{13} (δ_{23}) is the frequency of the transition $|1\rangle \to |3\rangle$ ($|2\rangle \to |3\rangle$), ω_{13} (ω_{23}) is the frequency of the light coupled to $|1\rangle \to |3\rangle$ ($|2\rangle \to |3\rangle$), and $m_1 = -1$ ($m_2 = 1$) is the magnetic quantum number of $|1\rangle$ ($|2\rangle$). We note that this detuning Δ_0 can be tuned by the optical frequencies; thus, the magnetic induction intensity B does not play any direct role in creating quantum nonreciprocity in our study.

If $|\Delta_0|$ is large enough, the phases of the two spin waves are not synchronized, resulting in a reduced efficiency in mutual coherence stimulation between the two channels, as reported in Ref. [S5]. Consequently, the two noise spectra are offset away from the Larmor frequency and become dispersive-like, accompanied by a drop of the contrast and broadening of the narrow peak. These effects together reduce the Gaussian discord. When $|\Delta_0|$ is smaller than Γ, the system is in the unbroken regime, and the frequencies of the two spin waves are pulled together, giving rise to a relatively larger discord generated by the operation of the non-Hermitian parametric-amplifier.

S.2 Modelling the coupling between the two channels in the Rubidium Vapor

We consider two channels which are dissipatively coupled to each other via atoms in thermal motion. In the forward case (Fig. **S1a**), the atoms "see" the same chirality for the beams having the same polarization and propagating in the same direction in CH1 and CH2. In this case, one atomic spin excitation $\hat{J}^{\dagger}$ ($|2\rangle \to |1\rangle$) in CH1 is accompanied by a lower sideband photon annihilation ($|2\rangle \to |3\rangle$) locally, represented as $\hat{H}_1 \propto \hat{a}_1 \hat{J}^{\dagger} + h.c.$ This excitation may diffuse to

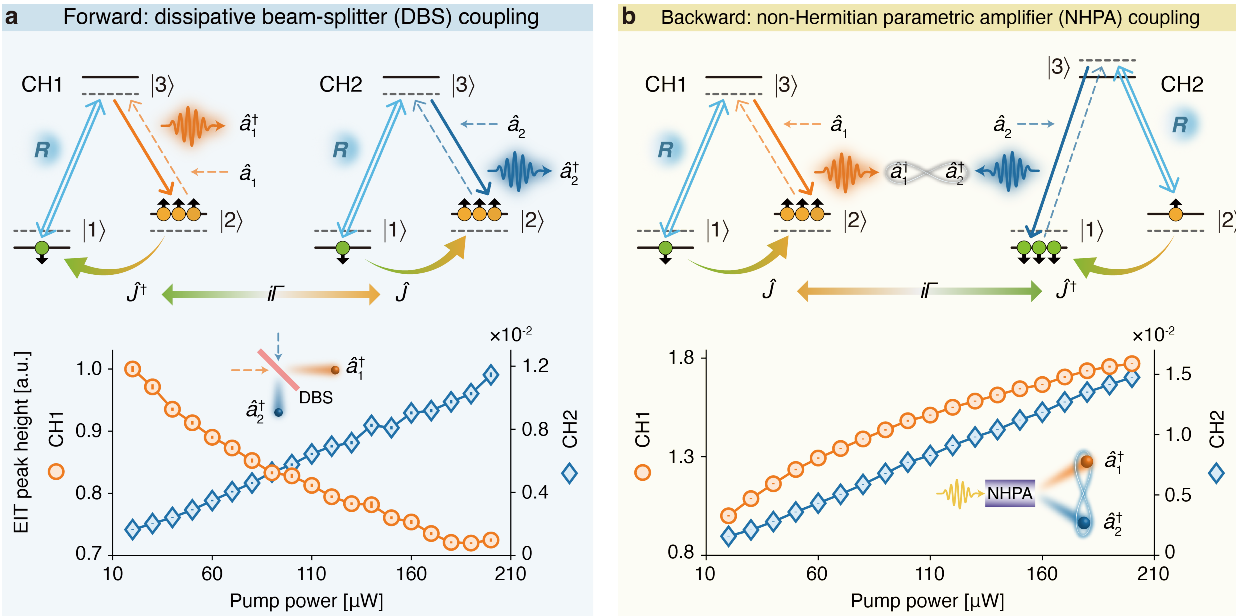

Fig. S1| Propagation-direction-dependent interactions between two channels. a, Schematics of the three-level Λ energy level in each channel. The ground states $|1\rangle$ and $|2\rangle$ are Zeeman sublevels of $|F = 2\rangle$, and the excited state $|3\rangle$ is $|F' = 1\rangle$ of the ^{87}Rb D1 line. An effective linear dissipative beam-splitter (DBS) interaction is achieved when the two light beams with same right circular polarizations propagate along the same direction. **b**, A non-Hermitian parametric-amplifier (NHPA) coupling is realized by reversing the input direction of the light in CH2. The lower panels of **a** and **b** show the electromagnetically induced transparency (EIT) response amplitudes in CH1 (orange circle) and CH2 (blue square) when the control power in CH2 is varied. For the dissipative beam-splitter coupling, the amplitude in CH1 decreases with increasing amplitude in CH2. For the non-Hermitian parametric-amplifier coupling, both of amplitudes in CH1 and CH2 increase.

the dark region outside the beam into the reservoir resulting in dissipation or to CH2 where it interacts with a light of the same polarization. In the latter case, the photon in the lower sideband ($|3\rangle \rightarrow |2\rangle$) is forward scattered along with the annihilation of the same spin excitation $\hat{J}$ ($|1\rangle \rightarrow |2\rangle$), described by $\hat{H}_2 \propto \hat{a}_2^\dagger \hat{J} + h.c.$

Thanks to the collective effect buildup along the propagation direction of light, this two-step interaction results in a linear dissipative beam-splitter (DBS) coupling between the two channels, which is dictated by $\hat{H}_D \propto a_1 \hat{a}_2^\dagger - \hat{a}_1^\dagger a_2$, and hence no quantum correlation emerges.

In contrast, in the backward case (Fig. **S1b**), the atoms "see" the opposite chirality for the beams having the same polarization but propagating in opposite directions in CH1 and CH2. In this case, a photon in the lower sideband ($|3\rangle \rightarrow |2\rangle$) is scattered in CH1 along with the annihilation of a spin excitation $\hat{J}$ ($|1\rangle \rightarrow |2\rangle$) captured by the Hamiltonian $\hat{H}_1 \propto \hat{a}_1 \hat{J}^\dagger + h.c.$ When it diffuses to CH2, in the reversed Λ-type EIT polarization configuration, this annihilation of the spin excitation $\hat{J}$ ($|1\rangle \rightarrow |2\rangle$) in CH1 is equivalent to the creation of a spin excitation $\hat{S}^\dagger$ ($|1\rangle \rightarrow |2\rangle$) in

CH2. Thus, in CH2 the control beam locally interacts with atoms, which results in the annihilation of a spin excitation $\hat{S}$ accompanied by the upper-sideband photon creation ($|3\rangle \rightarrow |1\rangle$) in CH2, as described by $\hat{H}_2' \propto \hat{a}_2^\dagger \hat{S} + h.c. = \hat{a}_2^\dagger \hat{J}^\dagger + h.c.$

Different from the forward case, this two-step interaction with collective dissipative coupling produces a nonlinear interaction, $\hat{H}_N \propto \hat{a}_1^\dagger \hat{a}_2^\dagger - \hat{a}_1 \hat{a}_2$, leading to the buildup of quantum correlations between the light (denoted by $\hat{a}_1^\dagger$ and $\hat{a}_2^\dagger$) in the channels. More details can be found in the following derivation.

In the forward case, by adiabatically eliminating the excited state, one can obtain the following coupled equations of two collective spin-wave excitations (or in short, spin waves) associated with the ground-state coherences, $\rho_{12}^{(1)}$ (in CH1) and $\rho_{12}^{(1)}$ (in CH2):

$$\begin{cases} \dot{\rho}_{12}^{(1)} = -\gamma_{12}'\rho_{12}^{(1)} + \Gamma_c \rho_{12}^{(2)} - \left[\Omega_c^{(1)*}\Omega_p^{(1)}\right]/\gamma_{23} \\ \dot{\rho}_{12}^{(2)} = -\gamma_{12}'\rho_{12}^{(2)} + \Gamma_c \rho_{12}^{(1)} - \left[\Omega_c^{(2)*}\Omega_p^{(2)}\right]/\gamma_{23} \end{cases}. \tag{S.3}$$

Here, γ_{12}' is the total effective decay rate of the ground-state coherence, γ_{23} is the decay rate of the coherence between states $|1\rangle$ and $|2\rangle$, Γ_c is the coupling rate of the ground-state coherences in the two channels, $\Omega_c^{(n)}$ and $\Omega_p^{(n)}$ are the resonance frequencies of the transition $|1\rangle \rightarrow |3\rangle$ and $|2\rangle \rightarrow |3\rangle$ in the channel n, respectively. For $\dot{\rho}_{12}^{(1)} = \dot{\rho}_{12}^{(2)} = 0$, the steady-state solutions are:

$$\begin{cases} \rho_{12}^{(1)} = B\left[-\gamma_{12}'\Omega_c^{(1)*}\Omega_p^{(1)} - \Gamma_c \Omega_c^{(2)*}\Omega_p^{(2)}\right] \\ \rho_{12}^{(2)} = B\left[-\gamma_{12}'\Omega_c^{(2)*}\Omega_p^{(2)} - \Gamma_c \Omega_c^{(1)*}\Omega_p^{(1)}\right] \end{cases}, \tag{S.4}$$

where $B = 1/[(\gamma_{12}'^2 - \Gamma_c^2)\gamma_{23}]$. The coherence ρ_{32} corresponding to the detected signal can be written as: $\rho_{32}^{(i)} = \left[i\Omega_c^{(i)}\rho_{12}^{(i)} + i\Omega_p^{(i)}\rho_{22}^{(i)}\right]/\gamma_{32}$, $dE^{(i)}/dz = i\bar{k}\chi^{(i)}E^{(i)}/2 = i\bar{k}N\mu_0\rho_{32}^{(i)}/2V\epsilon_0$, where ϵ_0 and μ_0 are the vacuum permittivity and permeability, respectively, $\bar{k}$ is the average wave vector, N is the number of atoms, V is the interaction volume, and $\chi^{(i)}$ is the atomic polarizability in channel i. Then, the coupling equations for the probe signals (i.e., the particular vacuum mode or the newly generated quantum signal) in the two channels are:

$$\begin{cases} \frac{dE^{(1)}}{dt} = \frac{A}{\gamma_{23}}\left\{-\Omega_p^{(1)}\left[1 - B\Omega_c^{(1)*}\Omega_c^{(1)}\gamma_{12}'\right] + \Omega_p^{(2)}B\Gamma_c\Omega_c^{(1)}\Omega_c^{(2)*}\right\} \\ \frac{dE^{(2)}}{dt} = \frac{A}{\gamma_{23}}\left\{-\Omega_p^{(2)}\left[1 - B\Omega_c^{(2)*}\Omega_c^{(2)}\gamma_{12}'\right] + \Omega_p^{(1)}B\Gamma_c\Omega_c^{(2)}\Omega_c^{(1)*}\right\} \end{cases}, \tag{S.5}$$

with $A = \left(Nc\bar{k}\mu_0\right)/2V\epsilon_0$, and the light speed c in the vacuum. Since the power of the control light is much greater than that of the probe signals, i.e., $\rho_{22} \approx 1$, the coupling equations is:

$$\begin{cases} dE^{(1)}/dt = -\gamma'' E^{(1)} + \Gamma_c'' E^{(2)} \\ dE^{(2)}/dt = -\gamma'' E^{(2)} + \Gamma_c''^{*} E^{(1)} \end{cases}, \tag{S.6}$$

with $\gamma'' = A\mu_0\left[1 - B\Omega_c^{(i)*}\Omega_c^{(i)}\gamma_{12}'\right]/\gamma_{23}$, $\Gamma_c'' = A\mu_0 B\Gamma_c\Omega_c^{(1)}\Omega_p^{(2)*}/\gamma_{23}$. Therefore, the effective interaction Hamiltonian in the forward case can be written as, with $g = -i\Gamma''^{*}$:

$$\hat{H}_D \propto \hbar(g a_1 a_2^{\dagger} - g^{*} a_1^{\dagger} a_2). \tag{S.7}$$

In the backward case, similar to the derivation in the forward case, the steady-state solutions of the ground state coherence are:

$$\begin{cases} \rho_{12}^{(1)} = B\left[-\gamma_{12}'\Omega_c^{(1)*}\Omega_p^{(1)} - \Gamma_c\Omega_p^{(2)*}\Omega_c^{(2)}\right] \\ \rho_{12}^{(2)} = B\left[-\gamma_{12}'\Omega_p^{(2)*}\Omega_c^{(2)} - \Gamma_c\Omega_c^{(1)*}\Omega_p^{(1)}\right] \end{cases}. \tag{S.8}$$

Note that, the probe signal in CH1 is still coupling to ρ_{23}, but the probe signal in CH2 is coupling to ρ_{13}: $\rho_{32}^{(1)} = \left[i\Omega_c^{(1)}\rho_{12}^{(1)} + i\Omega_p^{(1)}\rho_{22}^{(1)}\right]/\gamma_{32}$, $\rho_{13}^{(2)} = \left[-i\Omega_c^{(2)*}\rho_{12}^{(2)} - i\Omega_p^{(2)*}\rho_{11}^{(2)}\right]/\gamma_{32}$. Thus, the coupling equations for the probe signals in the two channels are:

$$\begin{cases} dE^{(1)}/dt = -\gamma'' E^{(1)} + \Gamma_c'' E^{(2)*} \\ dE^{(2)*}/dt = -\gamma'' E^{(2)*} + \Gamma_c''^{*} E^{(1)} \end{cases}. \tag{S.9}$$

The effective interaction Hamiltonian in the backward case is given by:

$$\hat{H}_N \propto \hbar(g a_1^{\dagger} a_2^{\dagger} - g^{*} a_1 a_2). \tag{S.10}$$

According to the multi-region model[S5, S6], we analyze the dynamics of the two-channel coupling by spin wave mixing, where the region of the atomic spin evolution is divided into three, labelled as dark (outside of the laser beams), bright 1 (CH1) and bright 2 (CH2). Associated spin states are denoted as $\hat{\sigma}^{(0)}$, $\hat{\sigma}^{(1)}$ and $\hat{\sigma}^{(2)}$, respectively. In the dark region, there is no light field, whereas in the bright regions, light fields with beam diameter of *d* are present. The time evolution of the system for these three regions is given by the coupled Heisenberg-Langevin equations:

$$\dot{\hat{\sigma}}^{(0)} = -\frac{i}{\hbar}\left[H_{\text{int}}^{0}, \hat{\sigma}^{(0)}\right] - \Gamma_{\text{rel}}^{(0)}\hat{\sigma}^{(0)} + S^{(0)} - (k_{02} + k_{01})\hat{\sigma}^{(0)} + k_{01}\hat{\sigma}^{(1)} + k_{02}\hat{\sigma}^{(2)} + \mathfrak{F}^{(0)}, \tag{S.11}$$

$$\dot{\hat{\sigma}}^{(1)} = -\frac{i}{\hbar}\left[H_{\text{int}}^{1}, \hat{\sigma}^{(1)}\right] - \Gamma_{\text{rel}}^{(1)}\hat{\sigma}^{1} + S^{(1)} - k_{10}\hat{\sigma}^{(1)} + k_{10}\hat{\sigma}^{(0)} + \mathfrak{F}^{(1)}, \tag{S.12}$$

$$\dot{\hat{\sigma}}^{(2)} = -\frac{i}{\hbar}\left[H_{\rm int}^{2}, \hat{\sigma}^{(2)}\right] - \Gamma_{\rm rel}^{(2)}\hat{\sigma}^{(2)} + S^{(2)} - k_{20}\hat{\sigma}^{(2)} + k_{20}\hat{\sigma}^{(0)} + \mathfrak{F}^{(2)}, \tag{S.13}$$

where $\Gamma_{\rm rel}^{(i)}$ $(i = 0, 1, 2)$ are the relaxation matrices accounting for the decays of the atoms, $S^{(i)}$ $(i = 0, 1, 2)$ are repopulations of atoms in the ground levels in the dark, bright 1, and bright 2 regions due to decays, respectively. Here, $\mathfrak{F}^{(i)}$ are the Langevin operators, which are characterized by $\left\langle \hat{f}_{uv}^{(i)}(z,t) \right\rangle = 0$ and

$$\left\langle \hat{f}_{uv}^{(i)}(z,t)\hat{f}_{\alpha\beta}^{(j)\dagger}(z',t') \right\rangle = \frac{L}{N} D_{\mu\nu i,\alpha\beta j}\delta(z-z')\delta(t-t'), \tag{S.14}$$

with the diffusion coefficients $D_{\mu\nu i,\alpha\beta j}$[S7]. Also, $k_{10(20)}$ are the hopping rates from bright 1 (2) to dark region, and $k_{01(02)}$ are the hoping rates from the dark region to bright 1 (2), which can be written as $k_{i0} = dN_i/(N_i dt)$, and $k_{0i} = dN_i/(N_0 dt)$, with $i = 1, 2$, and the atom numbers in the dark (N_0), bright 1 (N_1) and bright 2 (N_2) regions. Here, $k_{i0} = k \approx \bar{v}/d \sim 10^5\ \mathrm{s}^{-1}$, and $k_{0i} = k(d/D)^2 \sim 10^3\ \mathrm{s}^{-1}$, where D is the cell diameter, and $\bar{v}$ is the thermal velocity of the atomic motion. Since optical coherences decay much faster than the atomic hopping between the two channels, it is properly assumed that only ground-state coherences and populations in the two channels are effectively coupled through the thermal motion.

Here we take the non-Hermitian parametric amplifier as an example to illustrate the model in detail (Fig. S1). The spin dynamics in bright 1, bright 2, and dark regions are governed by the following Hamiltonian $H_{\rm int}^{0,1,2}$:

$$\hat{H}_{\rm int}^{0} = -\frac{\hbar N}{L}\int_0^L dz\left[-\Delta^{(0)}\hat{\sigma}_{33}^{(0)} - \delta^{(0)}\hat{\sigma}_{22}^{(0)}\right], \tag{S.15}$$

$$\hat{H}_{\rm int}^{1} = -\frac{\hbar N}{L}\int_0^L dz\left[-\Delta^{(1)}\hat{\sigma}_{33}^{(1)} - \delta^{(1)}\hat{\sigma}_{22}^{(1)} + g_1\hat{\sigma}_{32}^{(1)}\hat{a} + \Omega_1\hat{\sigma}_{31}^{(1)} + H.C.\right], \tag{S.16}$$

$$\hat{H}_{\rm int}^{2} = -\frac{\hbar N}{L}\int_0^L dz\left[-\Delta^{(2)}\hat{\sigma}_{33}^{(2)} - \delta^{(2)}\hat{\sigma}_{22}^{(2)} + g_2\hat{\sigma}_{31}^{(2)}\hat{b} + \Omega_2\hat{\sigma}_{32}^{(2)} + H.C.\right], \tag{S.17}$$

where $g = \mu\varepsilon/\hbar$ is the single-photon Rabi frequency with the transition dipole moment μ, and the electric field of a single photon $\varepsilon = \sqrt{\hbar\omega/(2\epsilon_0 V)}$[S8]. Here, $\Omega_i = \mu E_i/\hbar$ is the control laser Rabi frequency with the control laser electric field amplitude E_i. Here the atomic dipole operator at position z in the rotating frame is defined by locally averaging over a transverse slice containing many atoms

$$\hat{\sigma}_{\mu\nu}(z,t) = \lim_{\Delta z\to 0}\frac{L}{N\Delta z}\sum_{z<z_j<z+\Delta z}\hat{\sigma}_{\mu\nu}^{j}(z,t). \tag{S.18}$$

The Zeeman shift induced by the common bias magnetic field $\boldsymbol{B}$ and the frequency shift of the spin wave are denoted as δ_B and Δ_0, respectively, which contribute to various detunings in $H_{\text{int}}^{0,1,2}$:

$$\Delta^{(0)} = \frac{\delta_B}{2}, \qquad \delta^{(0)} = \delta_B, \tag{S.19}$$

$$\Delta^{(1)} = \frac{\delta_B}{2} + \Delta_0, \qquad \delta^{(1)} = \delta_B + \Delta_0, \tag{S.20}$$

$$\Delta^{(2)} = \frac{\delta_B}{2}, \qquad \delta^{(2)} = \delta_B - \Delta_0. \tag{S.21}$$

Since the control is much stronger than the probe, the populations $\hat{\sigma}_{11}^{(1)}, \hat{\sigma}_{22}^{(1)}, \hat{\sigma}_{11}^{(2)}, \hat{\sigma}_{22}^{(2)}$ and the coherences $\hat{\sigma}_{13}^{(1)}, \hat{\sigma}_{23}^{(2)}$ are mainly determined by the control fields. In this case, the nonlinear differential equations can be separated into two subsystems[S8]. In the first subsystem, the effect of the two quantum probe fields $\hat{a}, \hat{b}$ can be neglected, and these equations are solved in the steady state. The corresponding solutions are then injected into Eqs. (S.2-S.4), which determine the coherences $\hat{\sigma}_{23}^{(1)}, \hat{\sigma}_{31}^{(2)}, \hat{\sigma}_{21}^{(1)}, \hat{\sigma}_{21}^{(2)}$ as a function of $\hat{a}, \hat{b}^{\dagger}$.

In order to derive the quantum fluctuations of the light and the atoms, linearization around the steady state should be used:

$$\Sigma_1 = |\Sigma_1| + \delta\Sigma_1,\ \ \Sigma_1 = (\hat{\sigma}_{23}^{(1)}, \hat{\sigma}_{31}^{(2)}, \hat{\sigma}_{21}^{(1)}, \hat{\sigma}_{21}^{(2)}, \hat{\sigma}_{23}^{(0)}, \hat{\sigma}_{31}^{(0)}, \hat{\sigma}_{21}^{(0)})^T. \tag{S.22}$$

The first-order solution is determined by the equation:

$$(i\mathbb{I}\frac{\partial}{\partial t} + M_1)\Sigma_1 = S_1\hat{A} + i\hat{f}, \tag{S.23}$$

with Langevin operators

$$\hat{f} = (\hat{f}_{23}^{(1)}, \hat{f}_{31}^{(2)}, \hat{f}_{21}^{(1)}, \hat{f}_{21}^{(2)}, \hat{f}_{23}^{(0)}, \hat{f}_{31}^{(0)}, \hat{f}_{21}^{(0)})^T. \tag{S.24}$$

The mean value of Σ_1 is derived as $|\Sigma_1| = M_1^{-1}S_1\langle\hat{A}\rangle$. For the Fourier-transformed quantum fluctuations, one can obtain:

$$\delta\Sigma_1 = (M_1 + \omega\mathbb{I})^{-1}S_1\delta\hat{A} + i(M_1 + \omega\mathbb{I})^{-1}\hat{F}. \tag{S.25}$$

The Maxwell wave equations for σ_+ and σ_- polarized quantum fields $\hat{A} = (\hat{a}, \hat{b}^{\dagger})^T$ are given by:

$$\left(\frac{\partial}{\partial t} + c\frac{\partial}{\partial z}\right)\hat{A}(z,t) = igNT\Sigma_1(z,t), \tag{S.26}$$

where c is the speed of light, and N is the total atom number. The associated propagation matrix for the quantum-field in the frequency domain is obtained as

$$\delta\hat{A}(\omega, L) = \exp[M(\omega)L]\big(\delta\hat{A}(\omega, 0) + \hat{F}_L\big), \tag{S.27}$$

with the matrices

$$M(\omega)=i\frac{g^2N}{c}\boldsymbol{T}(M_1+\omega\mathbb{I})^{-1}S_1,\qquad \hat{F}_L=\int_0^L \exp[M(\omega)L]M_F(\omega)\hat{F}(z,\omega)dz, \quad (S.28)$$

where

$$\boldsymbol{T}=\begin{pmatrix}1 & 0 & 0 & 0 & 0 & 0 & 0\\ 0 & -1 & 0 & 0 & 0 & 0 & 0\end{pmatrix},\qquad M_F(\omega)=-\frac{gN}{c}\boldsymbol{T}(M_1+\omega\mathbb{I})^{-1}. \quad (S.29)$$

The Langevin atomic forces f are characterized by their diffusion coefficients matrix, which can be calculated using the generalized Einstein relation[S7].

(a) Gain in non-Hermitian nonlinear parametric processes

Defining

$$\exp[M(\omega)L]=\begin{pmatrix}A(\omega) & B(\omega)\\ C(\omega) & D(\omega)\end{pmatrix}, \quad (S.30)$$

we can rewrite Eq. (S.27) as follows,

$$\begin{pmatrix}\hat{a}(\omega,L)\\ \hat{b}^\dagger(\omega,L)\end{pmatrix}=\begin{pmatrix}A(\omega) & B(\omega)\\ C(\omega) & D(\omega)\end{pmatrix}\left[\begin{pmatrix}\hat{a}(\omega,0)\\ \hat{b}^\dagger(\omega,0)\end{pmatrix}+\begin{pmatrix}\hat{F}_a(\omega)\\ \hat{F}^\dagger_{b^\dagger}(\omega)\end{pmatrix}\right], \quad (S.31)$$

which allows us to represent the mean values $\langle\hat{A}\rangle$ and fluctuations $\delta\hat{A}$ of the output fields. When the mode $\hat{b}$ is the vacuum, $\langle\hat{b}_{\text{in}}\rangle$=0, it is observed that the probe field with mean value $\langle\hat{a}_{\text{in}}\rangle$ is amplified with gain $G_a=|A(\omega=0)|^2$, i.e.,

$$\langle\hat{a}_{\text{out}}\rangle=|A(\omega=0)|\langle\hat{a}_{\text{in}}\rangle. \quad (S.32)$$

(b) Noise spectrum of the correlated beams

Introducing the amplitude and phase quadratures of light as:

$$\hat{X}_c=\frac{1}{\sqrt{2}}(\hat{c}+\hat{c}^\dagger)\,,\qquad \hat{P}_c=\frac{1}{i\sqrt{2}}(\hat{c}-\hat{c}^\dagger), \quad (S.33)$$

with $\hat{c}=\hat{a},\hat{b}$, we can express the amplitude correlation and phase anti-correlation of the noise spectra S_{x-} and S_{p+} of the joint variables to be detected as follows:

$$S_{x-}2\pi\delta(\omega-\omega')\;=\;\frac{c}{L}\left\langle\left[\hat{X}_a(\omega)-\hat{X}_b(\omega)\right]\left[\hat{X}_a(\omega')-\hat{X}_b(\omega')\right]\right\rangle, \quad (S.34)$$

$$S_{p+}2\pi\delta(\omega-\omega')\;=\;\frac{c}{L}\left\langle\left[\hat{P}_a(\omega)+\hat{P}_b(\omega)\right]\left[\hat{P}_a(\omega')+\hat{P}_b(\omega')\right]\right\rangle. \quad (S.35)$$

Since our system utilizes warm atoms, the matrices M, M_F and $M_F\cdot D\cdot M_F^*$ should be modified as follows to take into account Doppler broadening:

$$M=\left(\frac{m}{2\pi k_BT}\right)^{\frac{1}{2}}\int_{-\infty}^{+\infty}M(v_z)\exp\left[-\frac{mv_z^2}{2k_BT}\right]dv_z, \quad (S.36)$$

$$M_F=\left(\frac{m}{2\pi k_BT}\right)^{\frac{1}{2}}\int_{-\infty}^{+\infty}M_F(v_z)\exp\left[-\frac{mv_z^2}{2k_BT}\right]dv_z, \quad (S.37)$$

$$M_F \cdot D^t \cdot M_F^* = \left(\frac{m}{2\pi k_B T}\right)^{\frac{1}{2}} \int_{-\infty}^{+\infty} M_F(v_z) \cdot D(v_z)^t \cdot M_F^*(v_z) \exp\left[-\frac{m v_z^2}{2k_B T}\right] dv_z, \qquad \text{(S.38)}$$

where we have used the Maxwell distribution function for the atomic velocity v_z, m is the mass of the ^{87}Rb atom, and k_B is the Boltzmann constant.

Note that, in the classical picture, the probe is a coherent state for the seed input with mean value $\langle \hat{a}_{in} \rangle \neq 0$ and $\langle \hat{b}_{in} \rangle \neq 0$. In contrast, in quantum nonreciprocity experiments, only control beams are applied in each channel, and the input probe is the vacuum, i.e. $\langle \hat{a}_{in} \rangle = \langle \hat{b}_{in} \rangle = 0$.

Regardless of whether we use the classical or quantum scenario, the quantum fluctuations of the input probe are the same, since both coherent state and vacuum state share the same variance of the quadratures $\mathrm{Var}(\hat{X}_i^{in})$ and $\mathrm{Var}(\hat{P}_i^{in})$ $(i = a, b)$.

In the framework of dissipative coupling, two spatially separated pump lights with circular polarizations interact with the atomic ensembles (input probes are vacuum), leading to the generation of the new quantum signals to be detected at the output, which fulfill the two-photon resonance condition.

S.3 Gaussian quantum discord

The concept of quantum discord was initially proposed as a measure of quantum correlation, more resilient to dissipative environments than quantum entanglement. Especially, Gaussian quantum correlations beyond entanglement can be captured by the measure of Gaussian discord. Entanglement is one type of strong quantum correlation, and “no entanglement “does not mean “no quantum correlation” [S9].

In the literature, for instance, in Ref. [S10] (highly cited paper), it is stated that “Quantum discord, a measure of genuinely quantum correlations… On pure states, quantum discord coincides with the entropy of entanglement. States with zero discord represent essentially a classical probability distribution embedded in a quantum system, while a positive discord, even on separable (mixed) states, is an indicator of quantumness”.

In Ref. [S11], it is stated that “The quantum discord D expands the concept of quantum correlations to include separable states. D > 0 indicates the presence of correlations that originate from the noncommutativity of quantum operators, which also applies to mixed states. Quantum discord has been shown to be a valuable resource for sensing, cryptography and quantum phase estimation and compared to entanglement, is expected to be more resilient to a dissipative bath”.

As a well-established measure, quantum discord can faithfully evaluate quantum correlations. In addition, we provide the values of Gaussian quantum discord with error bars in Fig. S2. The error bars are very small, which ensure that the quantum discord is nonzero.

Finally, we would like to provide more information about the factors that may limit the measured quantum discord.

(1) Beam size: Large beam size can increase the effective coupling rate between beams, which determines the Gaussian discord. But the overlap area between beams will also increase, which we do not want; so we choose proper beam diameters about 6 mm, which is large enough for high effective coupling rate and small enough to prevent significant overlap between the beams in the two channels.

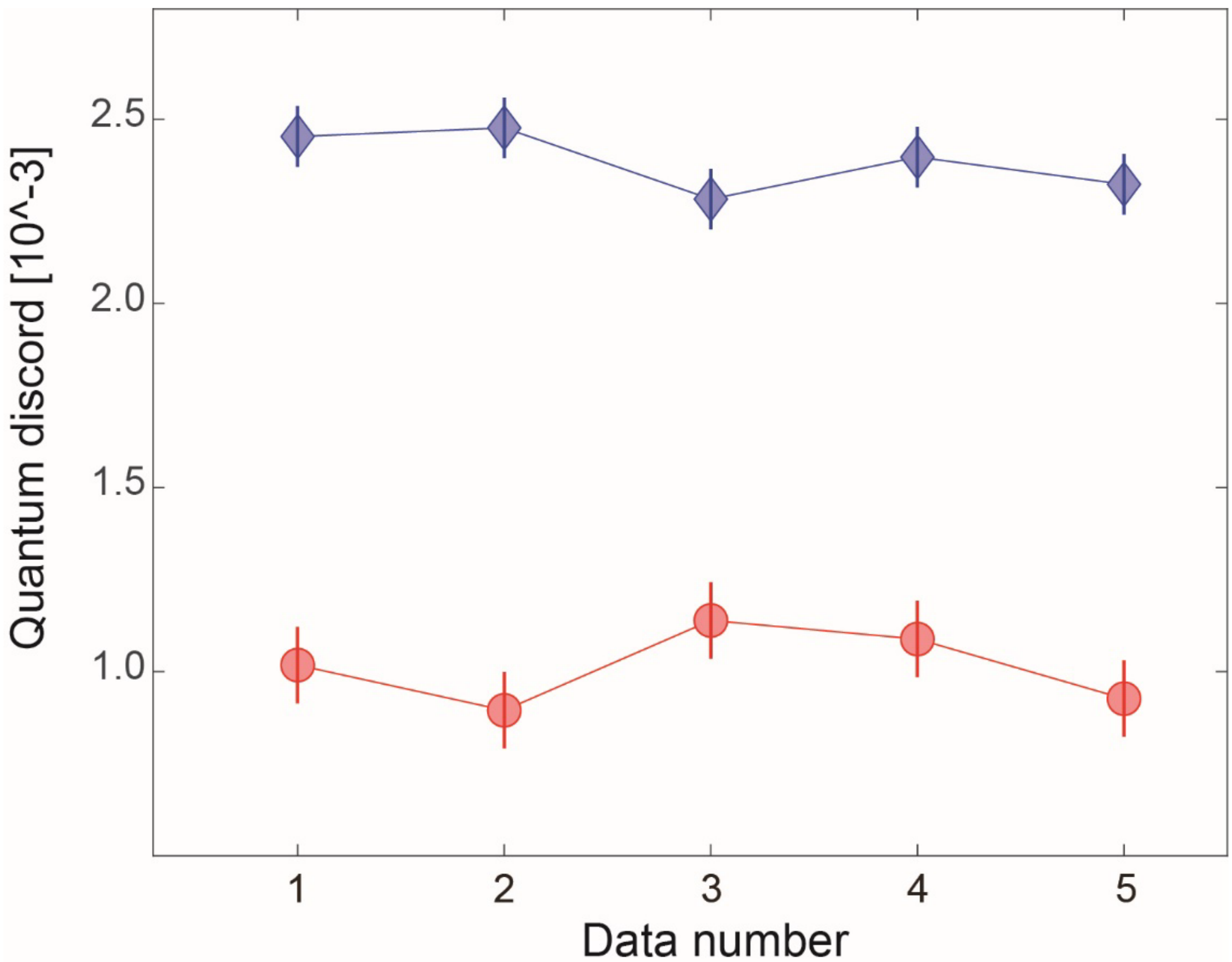

Fig. S2| Quantum discord. The measurement data are shown in this figure in five times of the cases in backward with same polarization (blue) and forward with different polarizations (red). The mean values are respectively 2.4×10^{-3} and 1.0×10^{-3}. The error bars are the standard deviations of each data, which represent s.d. from five measurements, and the values are 8.3×10^{-5} and 1.0×10^{-4}.

(2) Temperature: Temperature determines the density and mean velocity of the atoms, which influence the exchange rate of atoms between the two beams (i.e., channels). We need a larger atom density to obtain a larger quantum discord. However, temperatures above 70°C will affect the paraffin coating, and the atom-atom collision cannot be neglected in high temperature as well.

(3) The information remains in the reservoir: Some useful information will not be read out by the laser beams. The information remains in reservoir and has a lifetime of about 20 ms.

References

[S1] Fleischhauer, M. & Lukin, M. D. Dark-State Polaritons in Electromagnetically Induced Transparency. *Phys. Rev. Lett.* **84**, 5094-5097 (2000).

[S2] Firstenberg, O., Shuker, M., Ron, A. & Davidson, N. Colloquium: Coherent diffusion of polaritons in atomic media. *Rev. Mod. Phys.* **85**, 941-960 (2013).

[S3] Duan, L.-M., Lukin, M. D. & Cirac, J. I. Long-distance quantum communication with atomic ensembles and linear optics. *Nature* **414**, 413-418 (2001).

[S4] Peng, P., Cao, W., Shen, C. Qu, W., Wen, J., Jiang, L. & Xiao, Y. Anti-parity-time symmetry with flying atoms. *Nat. Phys.* **12**, 1139-1145 (2016).

[S5] Cao, W., Lu, X., Meng, X., Sun, J., Shen, H. & Xiao, Y. Reservoir-Mediated Quantum Correlations in Non-Hermitian Optical System. *Phys. Rev. Lett*. **124**, 030401 (2020).

[S6] Rochester, S. M. *Modelling Nonlinear Magneto-optical Effects in Atomic Vapors*. Ph.D. thesis, UC Berkeley (2010).

[S7] Davidovich, L. Sub-Poissonian processes in quantum optics. *Rev. Mod. Phys.* **68**, 127-173 (1996).

[S8]. Glorieux, Q. *et al*., Double-Λ microscopic model for entangled light generation by four-wave mixing. *Phys. Rev. A* **82**, 033819 (2010).

[S9] Modi, K., Brodutch, A., Cable, H., Paterek, T., and Vedral, V. The classical-quantum boundary for correlations: Discord and related measures. *Rev. Mod. Phys.* **84**, 1655, (2012).

[S10] Adesso, G., and Datta, A. Quantum versus Classical Correlations in Gaussian States. *Phys. Rev. Lett.* **105,** 030501 (2010).

[S11] Fink, J. M. et al., Stationary entangled radiation from micromechanical motion. Nature 570, 480-483 (2019).